CHINA FOUNDRY Research & Development
Vol. 20 No. 1 January 2023
www.springer.com/41230
https://doi.org/10.1007/s41230-023-1108-8

Effect of wide-spectrum pulsed magnetic field on grain refinement of pure aluminium

Ya-ming Bai[1], Gang Li[1], Ya-wei Sun[1], *Yong-yong Gong[1, 2], and Qi-jie Zhai[2, 3]

1. College of Science, Shanghai University, 99 Shangda Road, Shanghai 200444, China

2. Center for Advanced Solidification, Shanghai University, 99 Shangda Road, Shanghai 200444, China

3. School of Materials Science and Engineering, Shanghai University, 99 Shangda Road, Shanghai 200444, China

Abstract: A wide-spectrum pulsed magnetic field (WSPMF) was obtained by adjusting the number of current pulses and the pulse interval between adjacent pulses. The effect of WSPMF on the grain refinement of pure aluminium was studied. The distribution of electromagnetic force and flow field in the melt under the WSPMF was simulated to reveal the grain refining mechanism. Results show that the grain refinement is attributed to the combined effect of the melt flow and oscillation under a WSPMF. When the pulse interval is 5 ms, the extreme value of electromagnetic force is the highest, and the size of the crystal nucleus is 0.35 mm. In the case of similar flow rates, the grain size gradually decreases as the pulse interval increases. The range of the harmonic frequency of the magnetic field gradually expands with the increase of the pulse interval, which can provide more energy for nucleation at the solid-liquid interface and promote nucleation.

Keywords: wide-spectrum pulsed magnetic field; forced flow; grain refinement; frequency components

CLC numbers: TG146.21 **Document code:** A **Article ID:** 1672-6421(2023)01-040-09

1 Introduction

In the field of electromagnetic processing technology, the pulsed magnetic field (PMF) is an effective method for refining grains, reducing the segregation of solute elements, and improving the mechanical properties of cast alloys [1-4]. The influence of PMF on grain refinement has been investigated in recent decades. For instance, Wang et al. [5, 6] deduced that the grain refinement resulting from PMF was caused by an electromagnetic vibrating force and Joule heat effect in the melt. Yang et al. [7, 8] proposed that melt vibration and convection upon exposure to a PMF contribute to heterogeneous nucleation and lead to an increase in nucleation. Gong et al. [9, 10] found that the solidification structure can be refined by pulsed magneto-oscillation (PMO) during the nucleation stage and the first half period of crystal growth, and the nucleus originated from the mould wall and surface of the melt. Edry et al. [11, 12] determined that, during the dendrite growth stage, the refinement under the action of PMO can be explained by dendrite fragmentation. PMO increased the melting point to above the melting temperature, and the effect on the grain size can be explained by the cavity activation model. Li et al. [13] and Bai et al. [14] considered PMF leads to a high nucleation rate with lowering energy barrier and the critical radius of nucleation, the effect of the pulsed magnetic field on the melt can be summarized as follows: (1) the pulsed magnetic field can increase the number of crystal nucleus; (2) the forced convection of the melt under the pulsed magnetic field is beneficial to the homogenization of the temperature and the preservation of the crystal nucleus.

However, the influence of the frequency components on the solidification process has been rarely reported. During the propagation of electromagnetic waves in molten metal, the frequency components of electromagnetic waves change owing to the skin effect. The entire solidification process of molten metal can be affected by the high- to low-frequency components of electromagnetic waves.

In this study, a wide-spectrum pulsed magnetic field (WSPMF) with different harmonic frequency components was obtained by adjusting the number of current pulses and the time interval between adjacent pulses. The effect of the WSPMF on the grain refinement of pure aluminium was investigated. Numerical simulation was conducted by using

***Yong-yong Gong**

Male, Ph.D, Professor. Research interests: Electromagnetic metallurgy, pulsed high current, strong magnetic field, metal solidification, welding solidification.

E-mail: gyy@shu.edu.cn

Received: 2021-09-24; Accepted: 2022-10-11

COMSOL Multiphysics software to explore the distribution of the magnetic field and flow field under the WSPMF. In addition, the influence of the frequency components on the refinement of the metal solidification structure was discussed on the basis of an analysis of the frequency spectrum at a constant flow velocity.

2 Experimental procedures

2.1 Experimental method

A schematic of the experimental apparatus is shown in Fig. 1. The experimental set-up consists of WSPMF control systems, an induction coil, an oscilloscope, a steel mould (Φ54 mm× 100 mm) and a stainless-steel screen mesh.

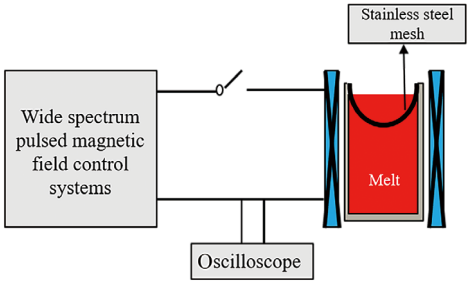

Fig. 1: Schematic diagram of experimental apparatus

The experimental parameters of this study are listed in Table 1. The electromagnetic parameters of the WSPMF include the current intensity (I), pulse interval (τ), discharge frequency ($1/T$), and pulse width of a single pulse (a).

Table 1: Electromagnetic parameters used in present experiment

No.	Peak current (A)	Frequency (Hz)	Pulse interval (ms)	Pulse width (ms)
1	0	0	0	0
2	2,500	1	25	10
3	2,500	1	20	10
4	2,500	1	15	10
5	2,500	1	10	10
6	2,500	1	6.7	10
7	2,500	1	5	10
8	2,500	1	3.3	10

Commercially pure aluminium was melted in an electric resistance furnace at 750 °C for 30 min. The molten metal was poured into a stainless-steel crucible with a steel screen mesh preheated to 400 °C, and WSPMF was applied immediately until the end of solidification. After the samples were cooled to room temperature, the specimens were cut along the central longitudinal section. The specimens were ground, polished, and etched by etchant solution ($HCl:HNO_3:HF:H_2O$=12:6:1:1). Finally, the macrostructure was observed by an Axio Imager A2m optical microscope and the average grain size was counted by the linear intercept method.

2.2 Numerical simulation model

2.2.1 Numerical procedure

A 2D axisymmetric mathematical model was established to couple the electromagnetic fields with fluid flow under WSPMF using COMSOL Multiphysics software. The geometric model is illustrated in Fig. 2. The melt radius is 27 mm and the height is 100 mm. Points A (27,50) and C (0,50) are located at the edge and centre of the melt, respectively. The Point B is used to indicate the distribution of electromagnetic force in the melt, and Point D is used to describe the flow of melt.

The governing equations for magnetic field and flow field were solved by COMSOL Multiphysics based on the finite element method. In the finite element mesh, the melt, coils, mold, air zone and infinite field were considered. Firstly, the actual current waveforms were measured by an oscilloscope under different electromagnetic parameters. Because the measured pulse current is a series of discrete data, the current waveforms after curve fitting are shown in the Fig. 3. The relevant physical properties of Al are listed in Table 2 [15]. The electromagnetic fields in a single period were calculated. Then, the coupling of the electromagnetic field with the fluid flow can be achieved by incorporating the Lorentz force into the Navier-Stokes equations.

The solidification under pulsed magnetic field is a complex process, some necessary assumptions are given as follows:

(1) The solidification system was cylindrical symmetry, a 2D axisymmetric mathematical model was established to solve the coupled problems between electromagnetic field and fluid field.

(2) The melt was regarded as the incompressible newton fluid.

(3) The influence of Joule heat was not considered in this model.

(4) The influence of the fluid flow on the magnetic field was neglected, because the magnetic Reynolds number is significantly smaller than unity in the molten melt [16].

(5) The influence of liquid level fluctuation on the melt flow field was not considered in the model.

Figure 3 shows three representative waveforms: (1) the pulse interval is greater than the pulse width (τ>10 ms); (2) the pulse interval is equal to the pulse width (τ=10 ms); and (3) the pulse interval is less than the pulse width (τ<10 ms). As shown in Fig. 3, the WSPMF has 10 pulses in one cycle, and the change

Table 2: Material properties of Al melt for numerical simulation [15]

Parameter	Value
Density, ρ (kg·m^{-3})	2,375
Liquidus temperature, T (K)	933.5
Electrical conductivity, σ_L (S·m^{-1})	8.2×10^{-6}
Dynamic viscosity, μ (Pa·s^{-1})	1.3×10^{-3}
Relative permeability	1
Relative permittivity	1

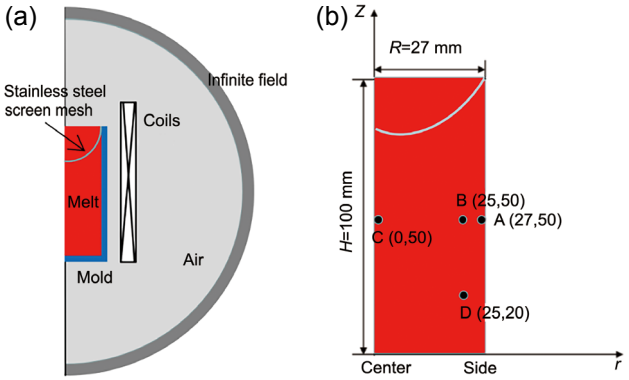

Fig. 2: Schematic diagram of numerical model: (a) two-dimensional axisymmetric model; (b) geometric model

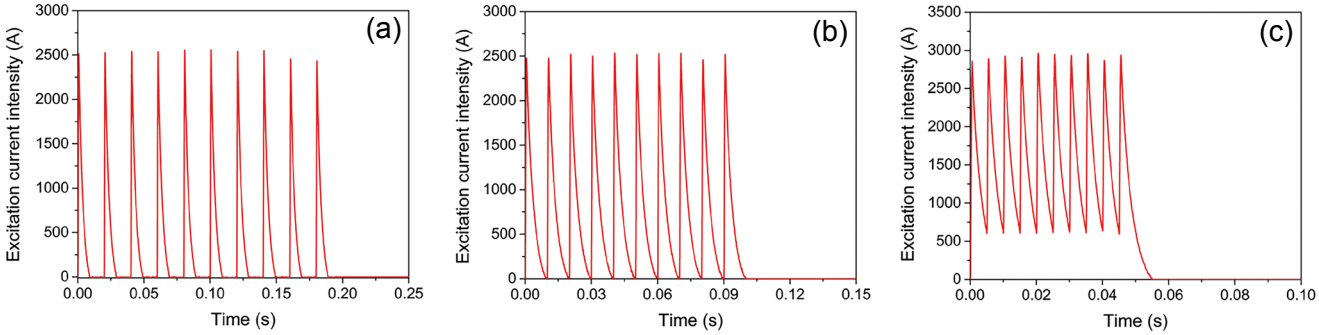

Fig. 3: Excitation current waveforms at different pulse intervals: (a) τ=20 ms; (b) τ=10 ms; (c) τ=5 ms

in the pulse time interval causes a significant change in the waveform of the magnetic field. When the pulse interval is greater than the pulse width (10 ms), a gap exists between adjacent pulses. The distance between adjacent pulses gradually decreases as the pulse interval decreases. When the pulse interval is less than the pulse width (10 ms), the superposition of the waveforms leads to an increase in the peak excitation current, and the waveform of the WSPMF changes significantly. The frequency component of the pulsed magnetic field is related to the waveform, and different waveforms contain different harmonic frequency components [17].

2.2.2 Governing equations

The electromagnetic field is governed by Maxwell's equations [18]:

$$\nabla \times H = J + \frac{\partial D}{\partial t} \quad (1)$$

$$\nabla \times E = -\frac{\partial B}{\partial t} \quad (2)$$

$$\nabla \cdot D = \rho_0 \quad (3)$$

$$\nabla \cdot B = 0 \quad (4)$$

where H is the magnetic field density, J is the current density, D is the electric flux density, t is the time, E is the electric field, B is the magnetic flux density, ρ_0 is electric charge density.

The corresponding constitutive equations are as follows:

$$J = \sigma E \quad (5)$$

$$B = \mu H \quad (6)$$

$$D = \varepsilon_0 E \quad (7)$$

where μ is the magnetic permeability, σ is the electric conductivity, ε_0 is the permittivity.

The induced magnetic field can be neglected because the magnetic Reynolds number $R_m \leq 1$ [19]. The Lorentz force F in the melt generated by the interaction of the induced current density J and the magnetic field is given by:

$$F = J \times B \quad (8)$$

In the present simulation, the standard k-ε model was used to model the turbulent kinetic energy and turbulent dissipation rate [20].

Conservation equation of mass:

$$\frac{\partial \rho}{\partial t} + \nabla \cdot (\rho U) = 0 \quad (9)$$

Conservation equation of momentum:

$$\frac{\partial (\rho U)}{\partial t} + \rho (U \cdot \nabla U) = \nabla \cdot \left[-pI + (\mu_0 + \mu_t) \left(\nabla U + (\nabla U)^T \right) \right] + G + P \quad (10)$$

where U is the flow velocity, G is the gravity, F is the Lorentz force, ρ is the density of the melt, μ_0 is the dynamic viscosity coefficient, $\mu_t = c_\mu k^2/\varepsilon$ is the turbulent viscosity coefficient.

Turbulent kinetic energy (k):

$$\frac{\partial (\rho k)}{\partial t} + \rho (U \cdot \nabla) k = \nabla \cdot \left[\left(\mu_0 + \frac{\mu_t}{\sigma_k} \right) \nabla k \right] + P_k - \rho \varepsilon \quad (11)$$

Turbulent dissipation rate (ε):

$$\frac{\partial (\rho \varepsilon)}{\partial t} + \rho (U \cdot \nabla) \varepsilon = \nabla \cdot \left[\left(\mu_0 + \frac{\mu_t}{\sigma_\varepsilon} \right) \nabla \varepsilon \right] + c_1 \frac{\varepsilon}{k} p_k - \rho c_2 \frac{\varepsilon^2}{k} \quad (12)$$

The production term is as follows:

$$P_k = \mu_t \left\{ 2\left[\left(\frac{\partial U_z}{\partial z} \right)^2 + \left(\frac{\partial U_z}{\partial z} + \frac{\partial U_r}{\partial r} \right)^2 \right] + \left(\frac{\partial U_z}{\partial z} + \frac{\partial U_r}{\partial r} \right)^2 \right\} \quad (13)$$

where c_1=1. 44, c_2=1. 92, σ_k=1. 0, σ_ε=1. 3, c_μ=0. 09 [21].

3 Results and discussion

3.1 Electromagnetic phenomena of WSPMF

The magnetic field distributions of the WSPMF at Point A (27,50) and Point C (0,50) of the melt with pulse intervals of 5 ms, 10 ms, 20 ms are shown in Fig. 4. When the pulse interval is greater than or equal to 10 ms, the magnetic flux density for pulse intervals of 10 ms and 20 ms at the edge does not change basically, the same is true at the centre. When the pulse interval is less than the pulse width, the current peak increases due to the superposition of the current waveforms, which leads to an increase in the magnetic flux density. During the propagation of the electromagnetic waves into the melt, the magnetic field has a phase difference between the edge and the centre of the melt, and the magnetic field waveform at the edge and centre changes significantly. The waveform of the magnetic field is related to its frequency component. The waveform changes during the propagation of the magnetic field, indicating that the frequency component of the magnetic field is changed.

When the pulse interval is 10 ms, the spectrum analysis of the WSPMF waveform at the edge and the centre is shown in the Fig. 5. The high frequency component of electromagnetic waves gradually decreases during the propagation of electromagnetic waves in the melt due to the dispersion effect. When the magnetic field propagates to the centre of the melt, the amplitude of the harmonic magnetic field with a frequency of 600 Hz is basically zero. According to the skin effect, the high-frequency harmonic frequency components of the magnetic field are concentrated near the mould wall. With the increase of electromagnetic field propagation distance to the inside of the melt, the high frequency components of the magnetic field gradually decrease.

The radial and axial electromagnetic force distributions at Point B (25,50) with pulse intervals of 5 ms, 10 ms, 20 ms are shown in Figs. 6(a) and (b), respectively. In comparison, axial electromagnetic force is two orders of magnitude smaller than radial electromagnetic force, so the effect of axial electromagnetic force on the melt is ignored. When the pulse interval is greater than or equal to the pulse width, the maximum radial electromagnetic force density in the $-r$ direction is 2.7×10^6 N·m^{-3}. When the pulse interval is 5 ms (shorter than the pulse width), the maximum radial electromagnetic force density in the $-r$ direction is 3.5×10^6 N·m^{-3}, which is more likely to promote the nucleus to fall off at the mold wall [19]. Multiple changes in the direction of the electromagnetic force in a cycle are more conducive to the oscillation of the melt, which promote the melt nucleation on the liquid surface and mold wall, and the nucleus falls off and drifts to the center and bottom of the melt under the multiple effects of electromagnetic force, gravity and flow, and finally form the phenomenon of crystal rain [22].

Figure 7 shows the statistical results of electromagnetic force density at the Point B (25,50) upon exposure to the WSPMF with pulse intervals ranging from 3.3 ms to 25 ms. When the pulse time interval is longer than the pulse width (10 ms), the mean value and the extreme value of the electromagnetic force density at different pulse time intervals do not change significantly. When the pulse time interval is shorter than the pulse width (10 ms), the mean value of the electromagnetic

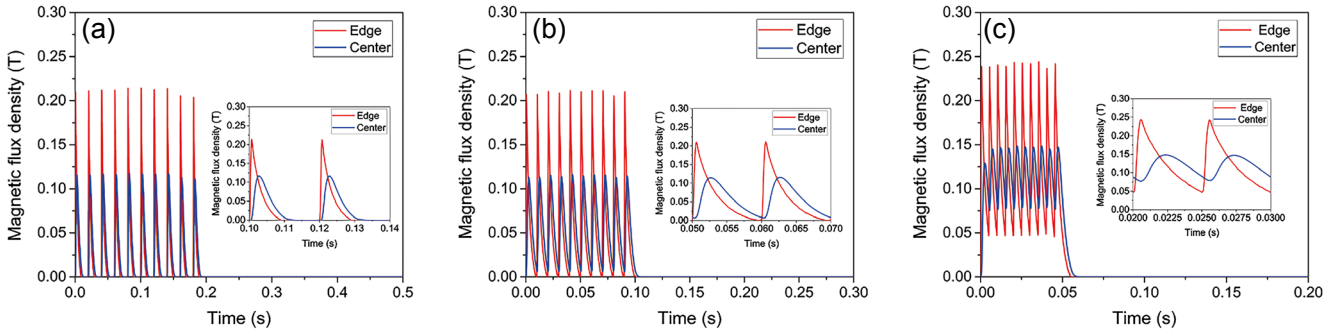

Fig. 4: Magnetic field distribution of WSPMF at the edge and centre of melt: (a) τ=20 ms; (b) τ=10 ms; (c) τ=5 ms

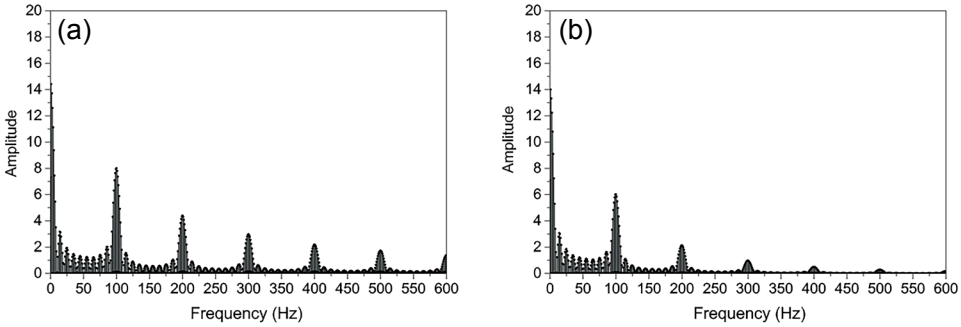

Fig. 5: Spectrum analysis of WSPMF waveform at edge (a) and centre (b) of melt when pulse interval is 10 ms

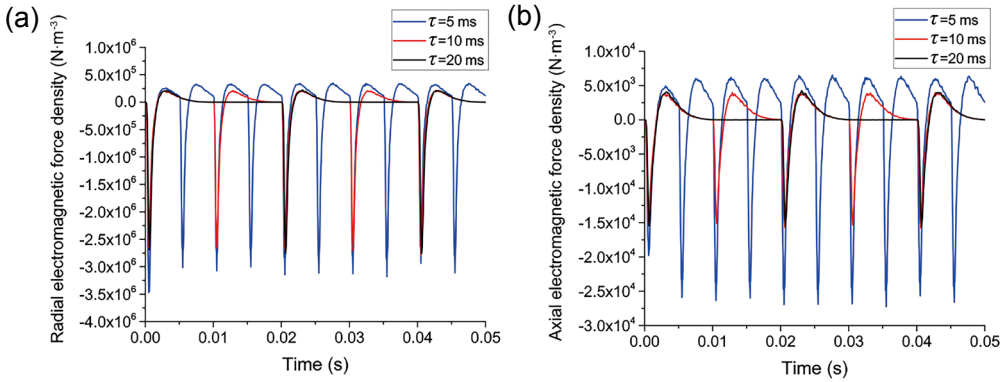

Fig. 6: Electromagnetic force distribution at Point B with time under different pulse time intervals: (a) radial electromagnetic force density; (b) axial electromagnetic force density

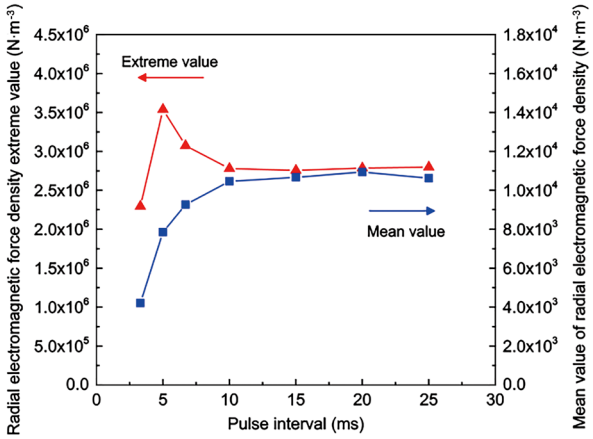

Fig. 7: Statistical results of electromagnetic force density at Point B (25,50)

force density gradually decreases with a decrease in the pulse interval. But the extreme value of the radial electromagnetic force is the largest when the pulse interval is 5 ms, which is easier to make nucleus fall off at the mold wall and enter the melt across the boundary layer, so as to proliferate the grains [19].

Forced convection under pulsed magnetic field is one of the key factors affecting grain refinement [7, 8]. The flow fields under the WSPMF with pulse intervals of 20 ms, 10 ms, and 5 ms are shown in Fig. 8. The flow pattern under the WSPMF is clearly similar to the double-loop flow pattern generated by the PMF [19]. However, owing to the barrier of the isolation net, two circulations are formed in the upper half of the melt. The maximum velocity is observed to appear at both sides of the vortexes.

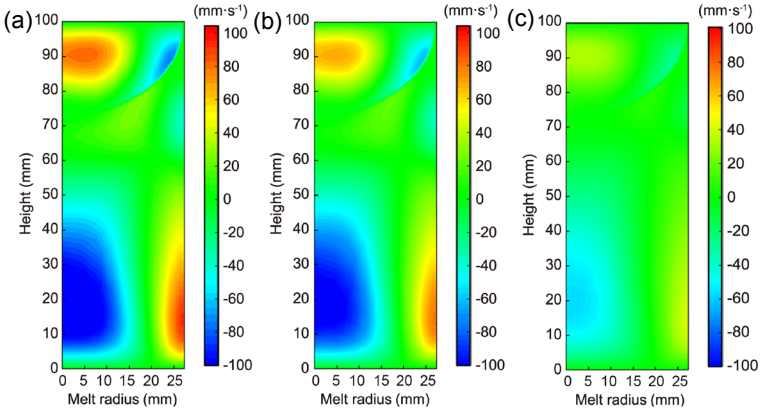

Fig. 8: Flow fields under WSPMF with different pulse intervals: (a) τ=20 ms; (b) τ=10 ms; (c) τ=5 ms

The variations in the velocity magnitudes at Point D (25,20) under the WSPMF are shown in Fig. 9 for different pulse intervals. The high frequency component of electromagnetic waves gradually decreases during the propagation of electromagnetic waves in the melt due to the dispersion effect. During the intermittent period, the viscosity of the melt and dissipation of turbulence gradually decrease the melt flow rate. The time-averaged velocity at Point D (25,20) with different pulse intervals is shown in Fig. 10. It is notable that the time-averaged velocity is approximately 0.12 m·s^{-1} when pulse interval is larger than 10 ms. In the case of pulse interval is shorter than 10 ms, the time-averaged velocity of the melt decreases as the pulse interval shortens.

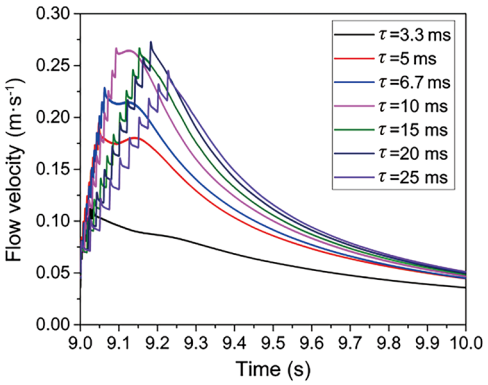

Fig. 9: Variation of velocity with time at Point D

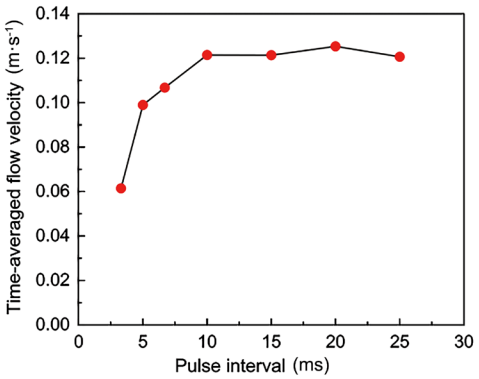

Fig. 10: Time-averaged velocity at Point D

3.2 Effect of pulse interval on solidification structure

The effect of different pulse intervals on the solidification structure of pure aluminium was studied. The longitudinal macrostructures of pure aluminium with and without exposure to a WSPMF are shown in Fig. 11. The solidification structure is a columnar structure without WSPMF, as shown in Fig. 11(a). After the WSPMF treatment, the columnar grains are transformed into equiaxed grains inside the solidified structure and above the screen mesh, as shown in Figs. 11(b)–(h). The average grain size of pure Al with different pulse intervals are shown in Fig. 12. Combined with the numerical simulation results in Fig. 7 and Fig. 10, when the pulse interval is 5 ms, the electromagnetic force density extreme is maximum, corresponding to a minimum average grain size of 0.35 mm. The flow rate and electromagnetic force extremes are basically similar during the increase of pulse interval from 10 ms to 25 ms, but the average grain size is gradually decreased with the increase of pulse interval.

When a WSPMF is applied to the melt, the electromagnetic force is generated by the interaction between the induced current generated in the molten metal and the pulsed magnetic field. The electromagnetic force is expressed as follows [22]:

$$F = J \times B = \frac{1}{\mu}(B\cdot\nabla)B - \frac{1}{2\mu}\nabla B^2 \tag{14}$$

The electromagnetic force can be resolved into a rotational component f_{rot} (first term) and an irrotational component f_{irrot} (second term). The rotational component will cause fluid motion, and the irrotational component can generate magnetic pressure on the melt. The ratio of the two determines the form of action of the electromagnetic force, whether it causes oscillation of the melt or promotes its flow. The ratio of f_{irrot} and f_{rot} can be expressed as follows [22]:

$$\frac{f_{irrot}}{f_{rot}} \approx \frac{L}{\delta} \tag{15}$$

where L is the characteristic length of the melt, which is related to the size of the melt. When the melt size does not change, the characteristic length of the melt does not change.

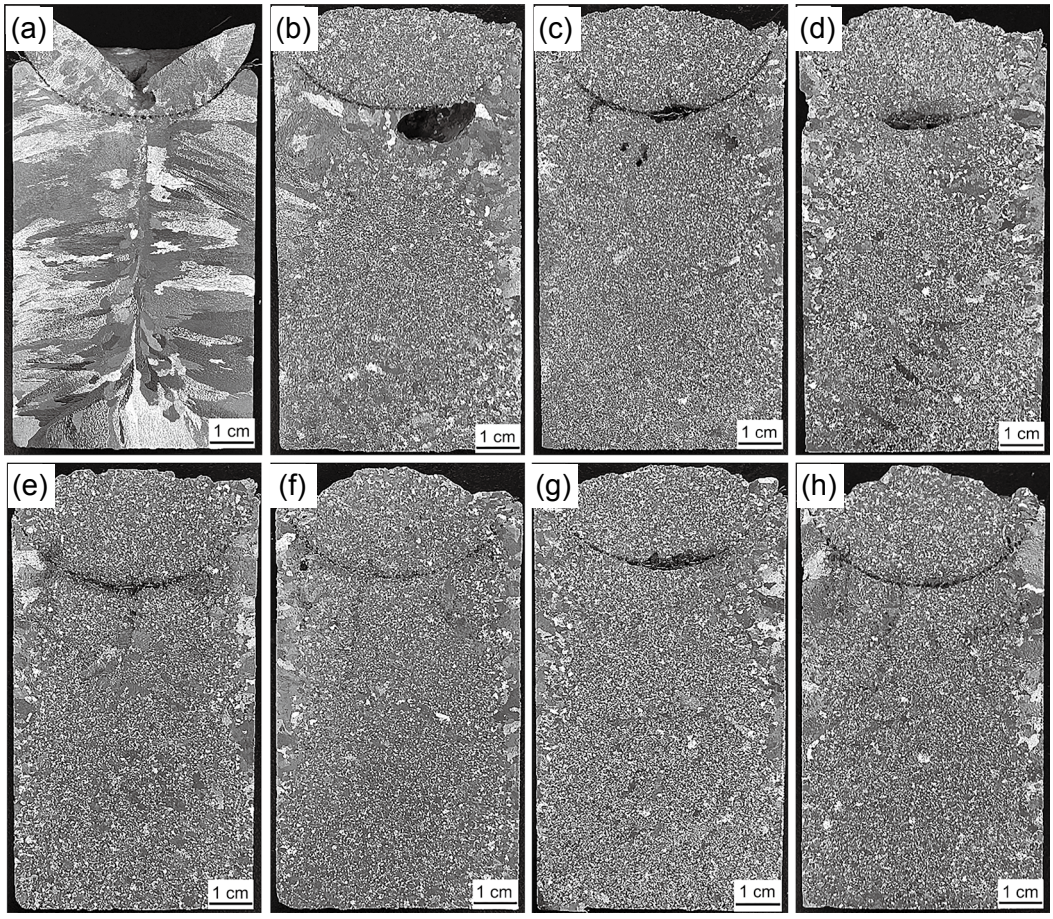

Fig. 11: Effect of pulse interval on the solidification structure: (a) untreated; (b) τ=3.3 ms; (c) τ=5 ms; (d) τ=6.7 ms; (e) τ=10 ms; (f) τ=15 ms; (g) τ=20 ms; (h) τ=25 ms

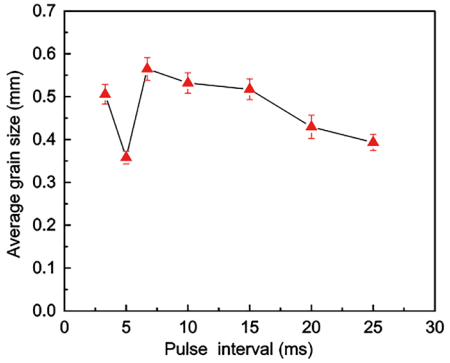

Fig. 12: Average grain size of equiaxed crystal

The skin depth δ can be expressed by Eq. (16):

$$\delta = \sqrt{\frac{2}{\omega\mu\sigma}} = \frac{1}{\sqrt{\pi f\mu\sigma}} \tag{16}$$

where ω is the angular velocity, f is the frequency.

According to the equation of skin depth, the electromagnetic wave with higher frequency has smaller skin depth. The Fourier transform of the pulse magnetic field waveform of the WSPMF for different pulse intervals produces the spectrum, as shown in Fig. 13. The frequency spectrum is composed of discrete spectral lines, and each spectral line represents a sine component. Each spectral line appears on an integer multiple of the fundamental frequency. The amplitude of each harmonic component of the spectrum gradually decreases with the increase of the harmonic frequency, and each peak represents the main harmonic frequency component.

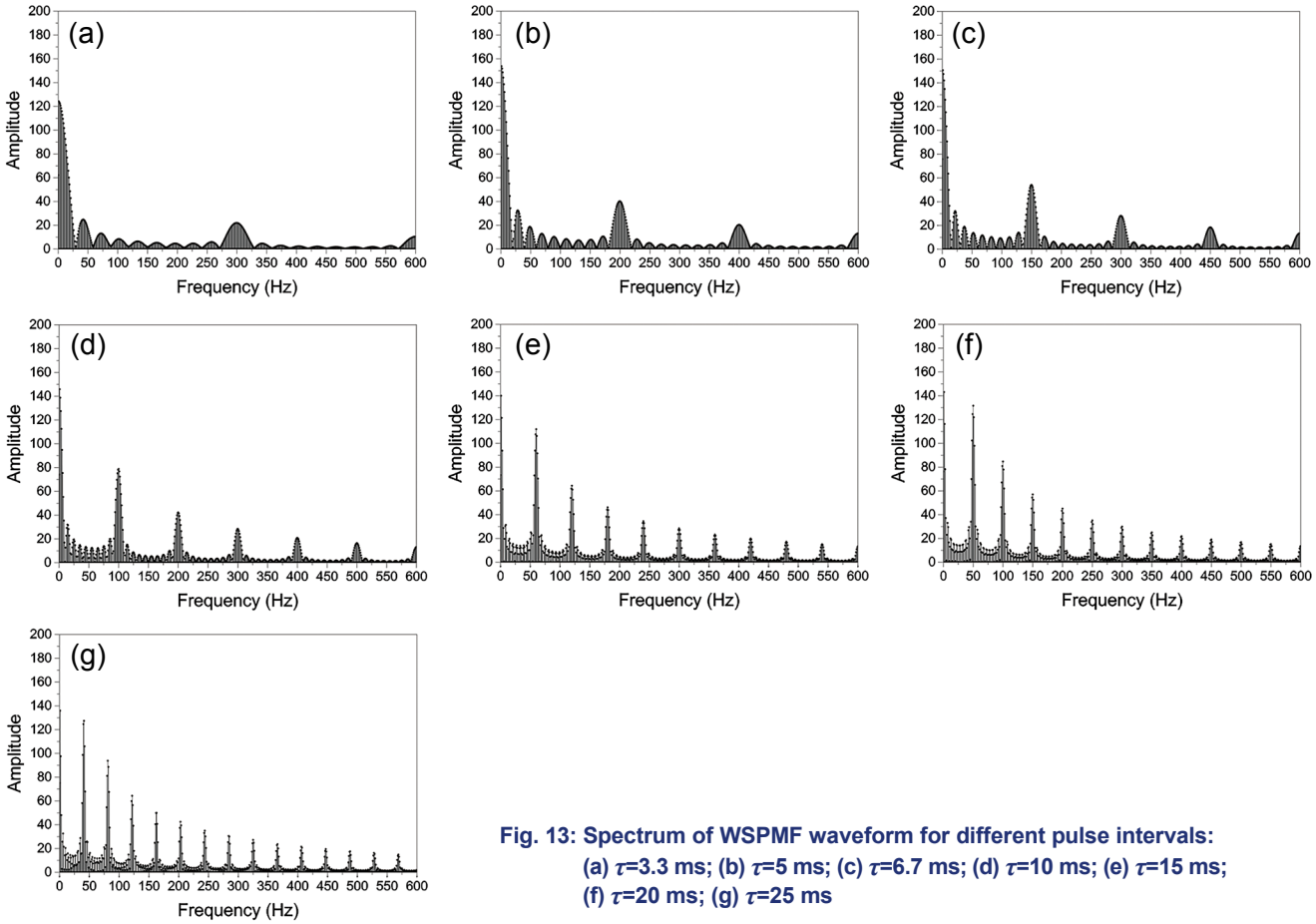

Fig. 13: Spectrum of WSPMF waveform for different pulse intervals: (a) τ=3.3 ms; (b) τ=5 ms; (c) τ=6.7 ms; (d) τ=10 ms; (e) τ=15 ms; (f) τ=20 ms; (g) τ=25 ms

From the spectrum of the WSPMF, it can be seen that as the pulse interval decreases, the frequency components of the magnetic field are dominated by higher harmonic frequencies, which will cause the skin depth to decrease. At the same time, the ratio of the characteristic length to the skin depth gradually increases, and the electromagnetic force works mainly as an irrotational force, which leads to a decrease in flow rate. Under the joint action of f_{irrot} and f_{rot}, the grain refinement effect becomes worse gradually with the decrease of pulse intervals. But the f_{irrot} of pulse interval (5 ms) is significantly greater than other pulse widths leads to the nucleus fall off at the mold wall and enter the melt across the boundary layer to promote grain refinement.

Figure 14 shows the distributions of the electromagnetic force in the melt when the pulse time interval is 5 ms. The radial electromagnetic force in $-r$ direction is expressed as the pressure on the melt, and in r direction is expressed as the pulling force on the melt, the radial electromagnetic force with alternating directions causes the melt to oscillate. When the pulse interval is 5 ms, the extreme value of the electromagnetic force density near the mold wall is the largest, which causes

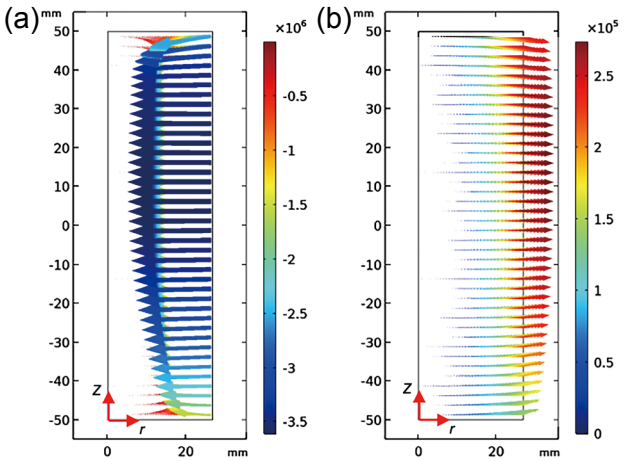

Fig. 14: Distribution of electromagnetic force in melt when pulse time interval is 5 ms: (a) maximum pressure force; (b) maximum pull force

the strongest melt oscillation. The crystal nucleus formed on the cold wall of the mold is broken off by the oscillating electromagnetic force and diffuses to the entire melt by the forced convection. As shown in Fig. 6, the electromagnetic force oscillates 10 times in one cycle, which is helpful for the crystal nucleus to break away from the mold wall and increase the nucleation. Moreover, the forced convection of the melt is conducive to the reduction of the temperature gradient [19] and the uniform temperature distribution, and improving the survival rate of crystal nucleus in the melt.

Furthermore, an interesting phenomenon is discovered in the experiment. When the pulse interval is greater than the pulse width, the extreme value and the time-average value of the electromagnetic force are basically unchanged, which means that the flow rate and the oscillation intensity are basically similar when the pulse interval is greater than the pulse width. However, the grain size gradually decreases as the pulse interval increases. Therefore, it is considered that the WSPMF has an important influence on the formation of crystal nucleus at the front of the solid-liquid interface.

According to thermodynamic theory, the Gibbs free energy changes when PMF is applied during the solidification of the melt. The change in the Gibbs free energy under a magnetic field can be expressed as [13]:

$$\Delta G = \Delta G_{\mathrm{v}} + \Delta G_{\mathrm{m}} \tag{17}$$

$$\Delta G_{\mathrm{m}} = -\frac{\Delta X^{\mathrm{L\text{-}S}} H^2}{2} \tag{18}$$

where ΔG_{v} is the free energy difference between the solid and liquid phases per unit volume, ΔG_{m} is the change in the free energy, and $\Delta X^{\mathrm{L\text{-}S}}$ is the change in the solid phase produced by the WSPMF. Under the action of the magnetic field, the change in the total Gibbs free energy and the critical radius for nucleation r^* is [13]:

$$\Delta G_{\mathrm{total}} = \frac{16\pi\sigma^3}{3\left(-\Delta G_{\mathrm{v}} + \left(\frac{-\Delta X^{\mathrm{L\text{-}S}} H^2}{2}\right)\right)^2} \tag{19}$$

$$r^* = \frac{2\sigma}{-\Delta G_{\mathrm{v}} + \left(\frac{-\Delta X^{\mathrm{L\text{-}S}} H^2}{2}\right)} \tag{20}$$

where σ is the surface free energy. Because ΔG_{v} is negative, $\Delta X^{\mathrm{L\text{-}S}}$ is positive. It can therefore be inferred that the critical nucleation energy $\Delta G_{\mathrm{total}}$ and critical radius r^* decrease as the magnetic free energy increases, which means the radius of critical nucleation decreases with the increase of magnetic energy loss.

From the spectrum analysis of the WSPMF in Fig. 13, as the pulse interval increases, the harmonic frequency components of the magnetic field are dominated by low-frequency components, and the energy attenuation gradually slows down. It can be seen from the skin effect that as the frequency of the magnetic field decreases, the skin depth increases. Figure 15 shows the skin depth of different harmonic frequency magnetic fields in pure aluminium melt. In the pure aluminium melt, the skin depth is about 1 cm when the harmonic frequency of the magnetic field is 100 Hz. The skin depth of the magnetic field increases from 1 cm to 1.5 cm when the harmonic frequency is reduced from 100 Hz to 40 Hz. From the spectrum analysis, it can be seen that when the pulse interval of the WSPMF is 25 ms, the low-frequency harmonic frequency is more abundant, and the range of the magnetic field is relatively large, which can provide energy for nucleation in more positions to reduce nucleation energy and nucleation radius to promote grain refinement.

The energy loss of the WSPMF in the melt with pulse intervals of 10 ms, 15 ms, 20 ms and 25 ms is shown in Fig. 16. With the increase of the pulse interval, the energy loss gradually increases, which indicates that the effective energy absorbed by the melt is increased. From the results of numerical simulation and solidification experiments, the forced convection and melt oscillation induced by the WSPMF play a vital role in the grain refinement. The oscillation of the melt is conducive to the generation of crystal nuclei, and the WSPMF with richer low frequency components can provide energy for the generation of crystal nuclei at more positions, thereby increasing the nucleation rate. In addition, the crystal nucleus diffuses to the entire melt under the flow field, which causes the homogenization of the solidified structure.

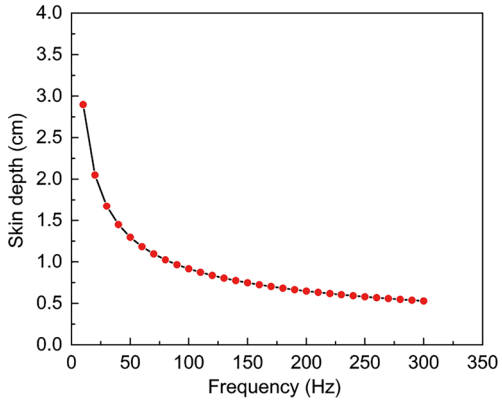

Fig. 15: Skin depth at different harmonic frequencies

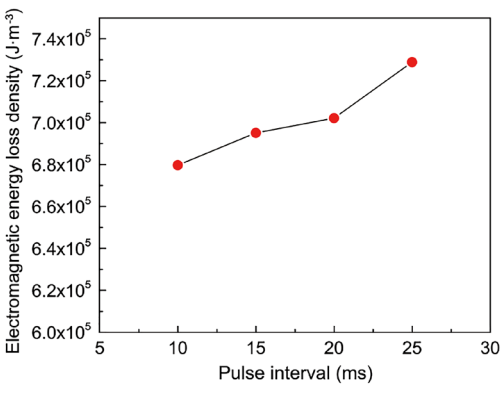

Fig. 16: Electromagnetic energy loss of WSPMF in melt with different pulse intervals

4 Conclusions

The effects of a wide-spectrum pulsed magnetic field (WSPMF) on the grain refinement of pure aluminium were investigated. The conclusions are summarized as follows:

(1) The experimental results show that the melt oscillation and flow under the WSPMF jointly affect the refinement of the solidified structure. The change in the frequency component of the WSPMF will cause the electromagnetic force in the melt to change, which will cause the melt to produce forced convection while changing the oscillation strength of the melt. When the pulse interval is smaller than the pulse width, the flow rate of the melt gradually decreases as the pulse interval decreases, but the electromagnetic force density near the wall has extreme values, and the melt oscillation intensity is the strongest at this time, which effectively enhances the refinement effect of the solidified tissue.

(2) The experimental results show that the frequency components of the WSPMF have significant effects on the solidification process of metals. Under the condition of similar flow rate, with the increase of pulse interval, the frequency component of the WSPMF is gradually dominated by low frequency harmonics, and the effective range of magnetic field harmonic effect is gradually expanded, which can provide energy for the formation of more nuclei at the solid-liquid interface and increase the nucleation rate in the melt to enhance the refining effect.

Acknowledgements

The work was financially supported by the National Natural Science Foundation of China (Grant Nos. 52071194, U1760204), and the National Key Research Program of China (Grant Nos. 2020YFB2008401 and 2017YFB0701800).

Conflict of interest

The authors declare that they have no conflict of interest.

References

[1] Li H, Liu S C, Jie J C, et al. Effect of pulsed magnetic field on the grain refinement and mechanical properties of 6063 aluminum alloy by direct chill casting. The Int. J. Adv. Manuf. Technol., 2017, 93(9–12): 3033–3042.
[2] Zhang Y H, Miao X C, Shen Z Y, et al. Macro segregation formation mechanism of the primary silicon phase in directionally solidified Al-Si hypereutectic alloys under the impact of electric currents. Acta Mater., 2015, 97: 357–366.
[3] Yin Z X, Gong Y Y, Li B, et al. Refining of pure aluminum cast structure by surface pulsed magneto-oscillation. J. Mater. Proc. Technol., 2012, 212(12): 2629–2634.
[4] Li Q S, Song C J, Li H B, et al. Effect of pulsed magnetic field on microstructure of 1Cr18Ni9Ti austenitic stainless steel. Mater. Sci. Eng. A, 2007, 466(1–2): 101–105.
[5] Wang B, Yang Y S, Zhou J, et al. Structure refinement of pure Mg under pulsed magnetic field. Mater. Sci. Technol., 2014, 27(1): 176–179.
[6] Wang B, Yang Y S, Sun M L. Microstructure refinement of AZ31 alloy solidified with pulsed magnetic field. Trans. Nonferrous Met. Soc. China, 2010, 20: 1685–1690.
[7] Li Y J, Teng Y F, Yang Y S, et al. Refinement mechanism of low voltage pulsed magnetic field on solidification structure of silicon steel. Met. Mater. Int., 2014, 20(3): 527–530.
[8] Yang Y S, Zhang K L, Li Y J, et al. Solidification structure control by the interaction of pulsed magnetic field and melt. Procedia Manuf., 2019, 37: 621–626.
[9] Gong Y Y, Luo J, Jing J X, et al. Structure refinement of pure aluminum by pulse magneto-oscillation. Mater. Sci. Eng. A, 2008, 497(1): 147–152.
[10] Liao X L, Zhai Q J, Luo J, et al. Refining mechanism of the electric current pulse on the solidification structure of pure aluminum. Acta Mater., 2007, 55(9): 3103–3109.
[11] Edry I, Mordechai T, Frage N, et al. Effects of treatment duration and cooling rate on pure aluminum solidification upon pulse magneto-oscillation treatment. Metall. Mater. Trans. A, 2016, 47(3): 1261–1267.
[12] Edry I, Frage N, Hayun S. The effect of pulse magneto-oscillation treatment on the structure of aluminum solidified under controlled convection. Mater. Lett., 2016, 182: 118–120.
[13] Li Y J, Tao W Z, Yang Y S. Grain refinement of Al-Cu alloy in low voltage pulsed magnetic field. J. Mater. Proc. Technol., 2012, 212(4): 903–909.
[14] Bai Q W, Ma Y L, Xing S Q, et al. Nucleation and grain refinement of 7A04 aluminum alloy under a low-power electromagnetic pulse. J. Mater. Eng. Perform., 2018, 27(2): 857–863.
[15] Li X B, Lu F G, Cui H C, et al. Migration behavior of solidification nuclei in pure Al melt under effect of current pulse. Trans. Nonferrous Met. Soc. China, 2014, 24: 192–198.
[16] Chen Q P, Shen H F. Numerical study on solidification characteristics under pulsed magnetic field. Int. J. Heat Mass Transfer, 2018, 120: 997–1008.
[17] He D P, Chen F, Shu G J, et al. Influence of vibrational disturbances of various wave patterns on dendrite growth. Journal of Synthetic Crystals, 1989, 18(4): 262–266.
[18] Ma X P, Yang Y S, Wang B. Effect of pulsed magnetic field on superalloy melt. Int. J. Heat Mass Transfer, 2009, 52(23): 5285–5292.
[19] Li B, Yin Z X, Gong Y Y, et al. Effect of temperature field on solidification structure of pure Al under pulse magnetooscillation. China Foundry, 2011, 8(2): 172–176.
[20] Jia Y H, Wang H, Le Q C, et al. Transient coupling simulation of multi-physical field during pulse electromagnetic direct-chill casting of AZ80 magnesium alloy. Int. J. Heat Mass Transfer, 2019, 143: 118524.
[21] Wang H, Jia Y, Le Q, et al. Transient numerical simulation of solidification characteristic under differential phase pulsed magnetic field. Comput. Mater. Sci., 2020, 172: 109261.
[22] Gong Y Y, Cheng S M, Zhong Y Y, et al. Influence of electromagnetic parameters on solidification structure of pure Al in the case of identical power. J. Iron Steel Res. Int., 2018, 25: 854–861.